Substrate Specificities of *Escherichia coli* Thioesterase I/Protease I/ Lysophospholipase L_1 Are Governed by Its Switch Loop Movement†

Yu-Chih Lo,‡ Su-Chang Lin,‡ Jei-Fu Shaw,§ and Yen-Chywan Liaw*,‡

Institute of Molecular Biology and Institute of Botany, Academia Sinica, Nankang, Taipei, Taiwan 115, ROC

Received September 2, 2004; Revised Manuscript Received November 28, 2004

ABSTRACT: *Escherichia coli* thioesterase I/protease I/lysophospholipase L_1 (TAP) is a multifunctional lysophospholipase and acyl-CoA thioesterase with a SGNH-hydrolase fold. The relationship between TAP's structure and its versatile substrate specificity, however, is unclear. Here, we present the crystal structure of TAP in complex with octanoic acid (TAP−OCA; OCA, a free fatty acid with eight carbon atoms, C_8). A structural comparison of native TAP with TAP−OCA reveals a remarkable conformational change in $loop_{75-80}$, called "switch loop movement", upon OCA binding to the substrate-binding crevice of TAP. OCA binding to the substrate-binding crevice results in a continuous hydrophobic surface, which triggers switch loop movement. The switch loop movement is acyl chain length dependent, with an effect of stabilizing the Michaelis complex (MC) of TAP during catalysis, and is essential for TAP's substrate preference. The finding of a sulfate ion binding site in the TAP structures, together with previous enzyme kinetic analyses, leads us to postulate that a putative CoA binding site is essential for efficient catalysis of thioesters in TAP. We also present the crystal structure of L109P−OCA (TAP's L109P mutant in complex with OCA), in which Leu109 mutated to Pro109 abolishes switch loop movement. This result strengthens our hypothesis that the switch loop movement is induced by hydrophobic interactions.

The enormous biotechnological potential of microbial esterases, proteases, and lipases has been extensively studied in the past two decades (*1*−*3*). The reactive products, generated by hydrolysis or synthesis, are ubiquitously used in pharmaceuticals, food sciences, and chemical industries (*1*−*3*). Structural studies on these enzymes have provided information leading to the elucidation of their substrate specificities, functions, and reactive mechanisms (*4*). *Escherichia coli* thioesterase I/protease I/lysophospholipase L_1 (TAP),[1] exhibiting versatile enzymatic activities, including the thioesterase, lysophospholipase, esterase, arylesterase, and protease activities, and stereoselectivity for amino acid derivatives (*5*−*10*), has been predicted to have industrial potential. There have been many enzymatic analyses of TAP reported. With regard to the thioesterase activity of TAP, it has been revealed that TAP preferentially catalyzes the hydrolysis of thioesters having an acyl chain longer than 10 carbon atoms (C_{10}), such as *cis*-vaccenyl-CoA ($\Delta^{11}C_{18:1}$), *cis*-palmitoleyl-CoA ($\Delta^{9}C_{16:1}$), and palmitoyl-CoA ($C_{16:0}$ or C_{16}-CoA) (*5*). The hydrolytic activity for thioesters having an acyl chain of 10 or fewer carbons was, however, not detected (*5*). By contrast, TAP shows higher activity for short or middle acyl chain ester derivatives and arylesters than for long acyl chain esters (*9*). With regard to lysophospholipase activity, TAP can hydrolyze monoacylglycerylphosphorylethanolamine, -glycerol, or -choline, especially those 1-acyllysophospholipids with acyl chain lengths of more than 14 carbons, but it cannot hydrolyze di- or triacylphospholipids (*11*). These results imply that the substrate binding or catalytic mechanism of TAP is quite complicated.

Recently, we have reported the tertiary structure of native TAP, which represents the first known structure of a multifunctional lysophospholipase (EC 3.1.1.5), and acyl-CoA thioesterase (EC 3.1.2.2), and identified it as a SGNH-hydrolase, which has the fourth identified tertiary fold utilizing a nucleophilic Ser, a His, and a carboxylic acid residue as a catalytic triad (*12*). To date, only four structures with the SGNH-hydrolase fold, TAP (*12*), SsEst (*13*), PAF-AH(Ib)α_1 (*14*), and RGAH (*15*), are known. A structural comparison of these four structures has revealed that a conserved hydrogen bond network stabilizes their catalytic centers and they may employ a unique catalytic mechanism different from those of most serine hydrolases (*12*). However, the detailed substrate binding and catalytic mechanisms of SGNH-hydrolases are poorly understood, which is in contrast to comprehensive investigations on serine hydrolases having the other three folds, the subtilisin-like fold, the trypsin-like fold, or the α/β-hydrolase fold. Therefore, structural studies on TAP in complex with different substrates are needed to improve our understanding of the substrate binding, substrate specificity, and catalytic mechanisms of SGNH-hydrolases.

† This work is supported by a grant from Academia Sinica to Y.-C. Liaw, Grants NSC 93-2320-B001-002 and NSC 92-2320-B001-008 to Y.-C. Liaw, and Grant NSC 85-2321-B001-017-A18 to J.-F.S. from the National Science Council, ROC.

* To whom correspondence should be addressed: Institute of Molecular Biology, Academia Sinica, Nankang, Taipei, Taiwan 115, ROC. Phone: (886)-2-2789-9199. Fax: (886)-2-2782-6085. E-mail: mbycliaw@gate.sinica.edu.tw.

‡ Institute of Molecular Biology.

§ Institute of Botany.

[1] Abbreviations: TAP, thioesterase I/protease I/lysophospholipase L_1; OCA, octanoic acid; MC, Michaelis complex; $C_{16:0}$-CoA, palmitoyl-CoA; DEP, diethylphosphono moiety; TAP−OCA, TAP in complex with OCA; L109P−OCA, TAP's L109P mutant in complex with OCA; C8-CoA, octanoyl-CoA.

10.1021/bi048109x CCC: $30.25
Published on Web 01/22/2005

Here we present the crystal structure of TAP in complex with octanoic acid (TAP−OCA; OCA, a free fatty acid with eight carbon atoms, C_8), in which OCA mimics the hydrolytic product of lysophospholipid/thioester/ester. A structural comparison of native TAP and TAP−OCA revealed a switch loop around the acyl chain-binding crevice of TAP, which plays an important role in stabilizing the TAP−substrate intermediates during catalysis. In addition, we also present the crystal structure of TAP's L109P mutant, a cloning artifact (*12*), in complex with OCA (L109P−OCA). Since the L109P mutant possesses an altered substrate specificity profile (*16*), structural differences between native TAP and its L109P mutant are examined in an attempt to elucidate the role of Leu109 during TAP's catalysis and the relationship between the L109P mutation and TAP's altered substrate specificity.

EXPERIMENTAL PROCEDURES

Protein Expression, Purification, Crystallization, and X-ray Data Collection. The expression, purification, crystallization, X-ray data collection, structure determination, and structural refinement statistics of native TAP and its L109P mutant have been fully described elsewhere (*12*). In this paper, we obtained two additional crystal structures, TAP−OCA and L109P−OCA. Crystals of the TAP−OCA and L109P−OCA complexes were obtained by soaking native TAP and L109P mutant crystals with 1.5 mM OCA for 4 h, respectively. The diffraction data of TAP−OCA crystals were collected using an ADSC Quantum 4 CCD detector on beamline 38B1 at the Super Photon ring-8 synchrotron radiation center in Japan. The diffraction data of the L109P−OCA crystals were collected using a MAC image plate detector on beamline 17B at the National Synchrotron Radiation Research Center (NSRRC) in Taiwan. All crystals were soaked in the solution containing 15% glycerol as a cryoprotectant. The data were integrated and scaled using the HKL package (*17*). Data collection statistics are given in Table 1.

Structural Determination, Refinement, and Model Quality. Using the native TAP structure (Protein Data Bank entry 1IVN) as a search model, the crystal structures of TAP−OCA and L109P−OCA were determined by molecular replacement (MR) as implemented in CNS (*18*). Structural refinement and automatic water searching were conducted with CNS using maximum likelihood and bulk-solvent correction. The model was adjusted and rebuilt with O (*20*). OCA was added to the TAP model using O, and the model was refined as described above. The geometric parameters were checked with PROCHECK (*19*). Coordinates and structural factors have been deposited in the Protein Data Bank, Research Collaboratory for Structural Bioinformatics, Rutgers University, New Brunswick, NJ, as entries 1U8U (TAP−OCA) and 1V2G (L109P−OCA).

RESULTS AND DISCUSSION

The recombinant His_6-tagged TAP and L109P mutant contain 190 residues. However, the final models of the TAP−OCA and L109P−OCA structures only contain 178 (82% of total residues) of 182 residues of TAP. Residues 179−182 of TAP and cloning artifact residues 183−190 were omitted because there were no interpretable electron density maps. Also, there are three flexible loops, residues 31−35 ($loop_{31-35}$), 75−80 ($loop_{75-80}$), and 111−120 ($loop_{111-120}$), as suggested by their high temperature factors (Figure 1) (*12*). Since there are 12 residues with uninterpretable electron density maps and 21 residues with high temperature factors, the TAP−OCA and L109P−OCA structures were refined to slightly higher *R* factors of 22.8 and 22.3%, respectively, for all data without a σ cutoff, of which 10% randomly distributed reflections were assigned to calculate R_{free} (25.9 and 26.3%, respectively). Refinement statistics appear in

Table 1: Data Collection and Refinement Statistics

	TAP−OCA	L109P−OCA
data collection		
space group	$P4_32_12$	$P4_32_12$
cell parameters (Å)	50.4, 50.4, 172.0	50.0, 50.0, 171.5
resolution range (Å)	19.78−2.08	24.8−2.0
no. of unique reflections (observed)	13812	14724
multiplicity	11.6	9.2
I/σ ratios[a]	15.3 (6.0)	12.1 (3.7)
completeness (%)[a]	96.4 (98.2)	97.1 (98.9)
R_{merge} (%)[a]	4.0 (25.0)	5.6 (43.7)
refinement		
R factor (%)/R_{free} (%)[b]	22.8/25.9	22.5/26.5
no. of non-hydrogen atoms		
protein	1413	1411
heterogeneous	38	20
water	112	107
rmsd for bond distances (Å)[c]	0.009	0.007
rmsd for bond angles (Å)[c]	1.3	1.1

[a] The values in parentheses refer to the I/σ, completeness, and R_{merge} of the highest-resolution shell: 2.08−2.17 and 2.00−2.09 Å for TAP−OCA and L109P−OCA, respectively. $R_{merge} = \sum|I_i - \langle I\rangle|/\sum|I_i| \times 100$. [b] *R* factor $= \sum|F_o - F_c|/\sum|F_o| \times 100$ for all available data. $R_{free} = \sum|F_o - F_c|/\sum|F_o| \times 100$ for a 10% subset of X-ray diffraction data omitted from refinement calculations. [c] Root-mean-square deviation from the ideal values calculated with CNS.

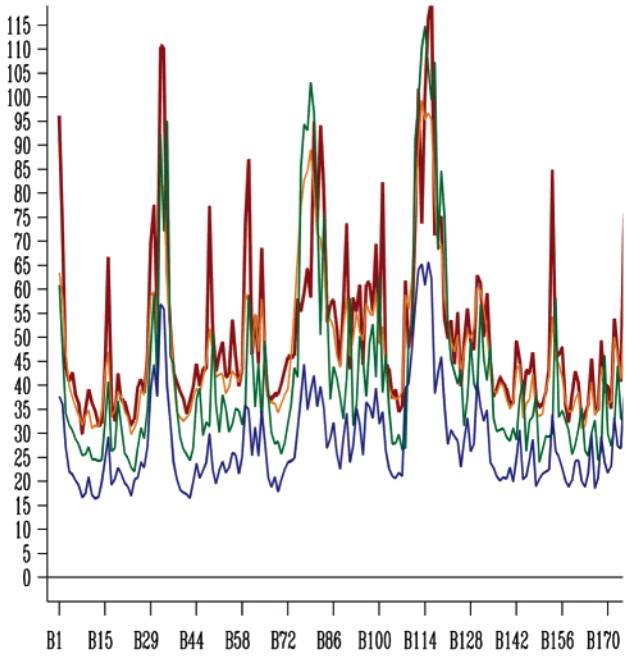

FIGURE 1: Plot of temperature factors along the polypeptide chain of native TAP, TAP−OCA, L109P, and L109P−OCA. The temperature factors of native TAP, TAP−OCA, L109P mutant, and L109P−OCA structures are shown in green, red, blue, and orange, respectively. This plot was generated using BPLOT (*25*).

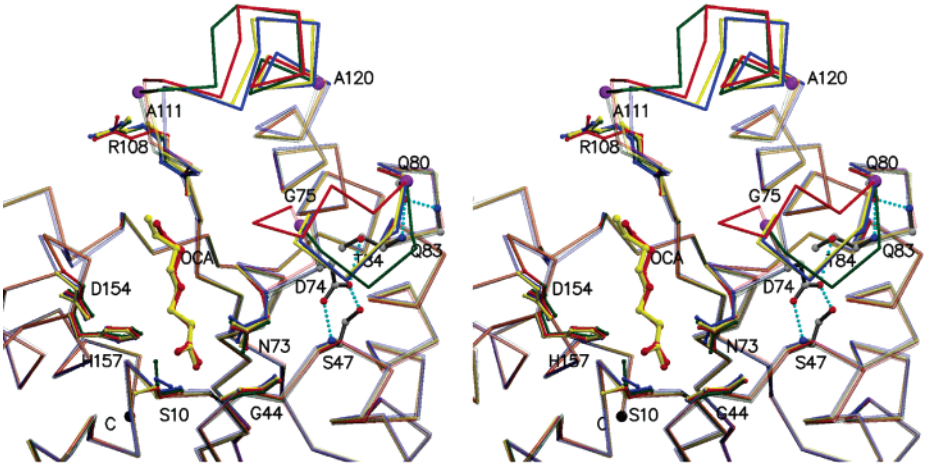

FIGURE 2: Structural comparison of native TAP, TAP−OCA, L109P, and L109P−OCA. The C^{α} traces of the superimposed native TAP, TAP−OCA, L109P, mutant, L109P−OCA structures are shown in green, red, blue, and yellow, respectively. The opaque C^{α} traces indicate two flexible loops, the switch loop and $loop_{111-120}$. The H-bonds restraining the N-terminus and C-terminus of the switch loop in the TAP structures are shown as cyan dotted lines. The catalytic triad, Ser10, Asp154, and His157, oxyanion acceptors, Ser10, Gly44, and Asn73, and OCA are presented as balls and sticks. This figure was generated using Raster3D (*26*).

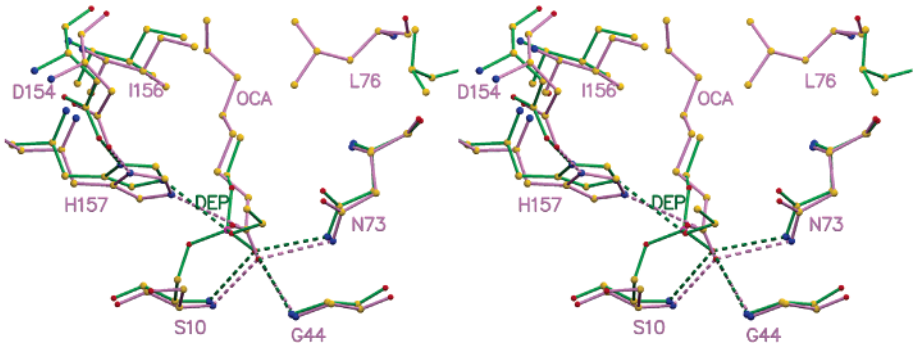

FIGURE 3: Stereo representation of the active sites of the TAP−OCA and TAP−DEP structures. Superimposition of the TAP−OCA and TAP−DEP structures was performed using four atoms, three C^{α} atoms of Ser10, Gly44, and Asn73 and the oxyanion atom of the substrate. The violet and green sticks represent the TAP−OCA and TAP−DEP structures, respectively. The dashed lines indicate the H-bonds between the oxyanion atom, the oxyanion acceptors, and the catalytic triad.

Table 1. The Ramachandran plot showed that more than 90% of the residues were in the most favored regions with no amino acids in disallowed regions.

Identification of a "Switch Loop". The crystal structure of native TAP, comprising a core of five parallel β-strands, flanked by seven α-helices and four 3_{10}-helices, has been reported (*12*). There are three flexible loops, $loop_{31-35}$, $loop_{75-80}$, and $loop_{111-120}$ (Figure 1) (*12*). Two of them, $loop_{75-80}$ and $loop_{111-120}$, are located in the vicinity of the substrate-binding crevice (Figure 2). To investigate the catalytic mechanism of TAP, we cocrystallized or soaked TAP crystals with the substrates or the substrate analogues of thioesterase, protease, lysophospholipase, or esterase, or fatty acids as hydrolytic products. TAP crystals soaked with OCA were the only crystals (TAP−OCA) obtained with diffraction quality.

In the TAP−OCA structure, OCA lodges in the expected substrate-binding crevice; its carboxylic group and the hydrocarbon moiety face the catalytic Ser10 and residue Arg108, respectively (Figure 2). The O^2 atom of the carboxylic group of OCA is hydrogen bonded to the nitrogen atoms of the oxyanion acceptors, including the amide groups (NH) of Ser10 and Gly44 and $N^{\delta 2}$ of Asn73, and its O^1 atom is hydrogen bonded to $N^{\epsilon 2}$ of the catalytic His157 of TAP (Figure 3). According to the position of OCA in TAP, the TAP−OCA structure may mimic a TAP−product complex.

Significantly, in the TAP−OCA structure, one of the aforementioned flexible loops, $loop_{75-80}$ (^{75}GLRGFQ^{80}), undergoes a remarkable conformational change and moves toward the substrate-binding crevice and $loop_{111-120}$ (Figure 2), and with an ordered electron density map in comparison to that of the native TAP structure, even their overall foldings are very similar with a root-mean-square derivation (rmsd) of 0.4 Å over 174 C^{α} atoms. Also, residues Gly72−Asp74 are folded as a part of a β-turn in native TAP, but together with residues Gly75 and Leu76, folded as a helix (named helix αD′) in the TAP−OCA complex, although residues Gly72−Asp74 do not have any movement. Notably, in all the TAP structures, Asp74 at the N-terminus of $loop_{75-80}$ is highly constrained by three H-bonds, including the Asp74 $O^{\delta 1}$−Ser47 O^{γ} bond, the Asp74 $O^{\delta 1}$−Thr84 $O^{\gamma 1}$ bond, and the Asp74 $O^{\delta 2}$−Ser47 NH bond (Figure 2). In addition, the C-terminus of $loop_{75-80}$ of all the TAP structures is restrained by Pro81 (Figure 2), which is a rigid residue because of its physical property, and by two hydrogen bonds, the Gln80 O−Gln83 NH bond and the Gln80 O−Thr84 NH bond. These results thus reveal that Asp74, Gln80, and Pro81 play significant roles in fastening both the N-terminus and the

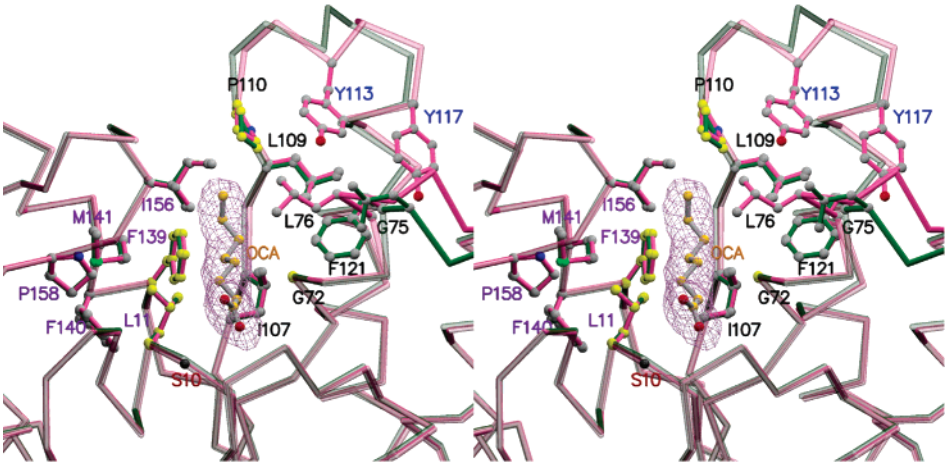

FIGURE 4: Structural comparison of native TAP and TAP−OCA around the substrate-binding crevice. The C^{α} traces of native TAP and TAP−OCA structures are shown in green and pink, respectively. The opaque C^{α} traces represent the switch loops of the TAP structures. The residues of the Leu11 and Pro110 hydrophobic clusters are labeled in purple and black, respectively, and presented as balls and sticks. The location of Ser10 is labeled in red. The carbon atoms of the residues in close contact with OCA are colored yellow. The $2F_o - F_c$ electron density map of OCA is countered at the 1σ level. The electron density map was created using MINIMAGE (*27*).

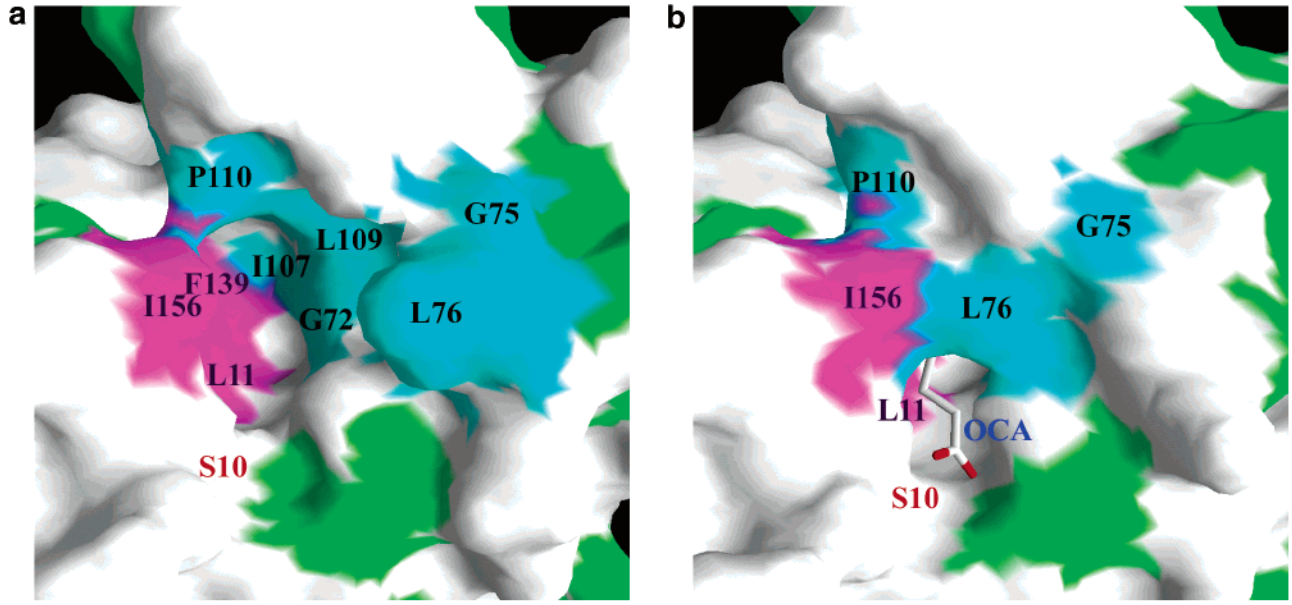

FIGURE 5: Comparison of the molecular surfaces of the native TAP and TAP−OCA structures around the substrate-binding crevice. (a) Surfaces of the Leu11 and Pro110 hydrophobic clusters of native TAP, shown in purple and cyan, respectively. (b) Continuous hydrophobic surface in the TAP−OCA structure. The surfaces of the other hydrophobic residues of the TAP structures are shown in green. This figure was prepared with GRASP (*28*).

C-terminus of $loop_{75-80}$, respectively, and also in controlling the movement of $loop_{75-80}$ upon substrate binding. Since the main chain NH group of Gln80 in the TAP−OCA structure shifts 0.88 Å compared to that of native TAP, Gln80 is thus involved in the movement of $loop_{75-80}$. Here, we designated this well-controlled $loop_{75-80}$ as a "switch loop".

TAP's Switch Loop Movement Is Acyl Chain Length Dependent. We have mentioned that the conformational change in TAP's switch loop results from the binding of OCA. However, in our previously reported TAP−DEP structure (*12*) (DEP, diethyl phosphono moiety, a serine hydrolase inhibitor), the binding of DEP does not induce a conformational change in the switch loop. The length of the ethyloxy moiety of DEP in TAP's substrate-binding crevice approximately corresponds to the length of a C_4 acyl chain (Figure 3), which is shorter than the C_8 acyl chain of OCA by four hydrocarbon atoms. This shows a lower hydrophobicity in the substrate-binding crevice of the TAP−DEP complex than in that of the TAP−OCA complex. These observations reveal that short acyl chain substrates could not trigger TAP's switch loop movement and suggest that switch loop movement is acyl chain length dependent.

Switch Loop Movement Is Triggered by Hydrophobic Interactions. In the native TAP structure, both flanks of the substrate-binding crevice are comprised of mainly hydrophobic residues, forming two separated hydrophobic clusters; one contains Leu11, Phe139, Phe140, Met141, Ile156, and Pro158 (named the Leu11 hydrophobic cluster), and the other contains Gly72, Gly75, Leu76, Ile107, Leu109, Pro110, and Phe121 (named the Pro110 hydrophobic cluster) (Figures 4 and 5a). Notably, in the TAP−DEP structure, the ethyloxy moiety of DEP is only in close contact with residues in the Leu11 hydrophobic cluster, not the Pro110 hydrophobic cluster. However, in the TAP−OCA structure, the C^3 and

Table 2: Close Contacts between OCA and Interacting Residues As Calculated with HBPLUS

ligand	residue	distance (Å)
OCA (C^1)	Asp9 (C^γ)	4.1
	Ser10 (C^α)	4.0
	Ser10 (C^β)	3.2
	Asn73 (C^γ)	3.7
OCA (C^2)	Asp9 (C^γ)	3.6
	Asn73 (C^γ)	3.6
OCA (C^3)	Leu11 (C^γ)	3.7
	Leu11 ($C^{\delta 2}$)	4.0
OCA (C^5)	Leu11 (C^γ)	4.0
	Leu11 ($C^{\delta 1}$)	3.6
	Gly72 (C^α)	4.0
OCA (C^6)	Gly72 (C^α)	3.6
	Gly72 (C)	4.1
OCA (C^7)	Phe139 (C^ζ)	3.9
OCA (C^8)	Pro110 (C^γ)	3.9
	Pro110 (C^δ)	3.6

Table 3: Close Contacts between Switch Loop and Interacting Residues As Calculated with HBPLUS

	residue	distance (Å)
Gly75 (C^α)	Leu109 ($C^{\delta 1}$)	3.7
	Leu109 ($C^{\delta 2}$)	3.9
	Tyr117 ($C^{\epsilon 2}$)	3.8
	Tyr117 (C^ζ)	3.8
	Phe121 ($C^{\epsilon 1}$)	4.0
Gly75 (C)	Leu109 ($C^{\delta 1}$)	3.8
	Leu109 ($C^{\delta 2}$)	3.7
	Tyr113 ($C^{\epsilon 2}$)	4.0
	Tyr117 ($C^{\epsilon 2}$)	3.8
Leu76 ($C^{\delta 1}$)	Pro110 (C^δ)	3.9
Leu76 (C^α)	Tyr113 ($C^{\epsilon 2}$)	3.5
	Tyr113 (C^ζ)	3.7
Leu76 (C)	Tyr113 ($C^{\epsilon 2}$)	3.7
	Tyr113 (C^ζ)	3.9
Leu76 (C^γ)	Tyr113 (C^ζ)	4.1
Leu76 ($C^{\delta 1}$)	Tyr113 ($C^{\epsilon 1}$)	4.0
	Tyr113 (C^ζ)	3.7

C^4 atoms of OCA are in close contact (<4.1 Å) with residues in the Leu11 hydrophobic cluster, while the C^5-C^8 atoms of OCA are in close contact with those in the Pro110 hydrophobic cluster (Table 2 and Figure 4; *21*, *22*). They form a continuous hydrophobic surface (Figure 5b), thereby increasing the hydrophobicity around the substrate-binding crevice of TAP. We postulate that hydrophobic interactions could be a predominant force triggering such a movement of the switch loop. Thus, not only a middle or long acyl chain substrate but a continuous hydrophobic surface is probably essential for switch loop movement.

Carefully examining the switch loop, we find Leu76, a hydrophobic residue on the switch loop, shows the largest movement when OCA binds to TAP. It moves toward Ile156 in the Leu11 hydrophobic cluster (Figure 5b), and the distance between them changes from 8.4 Å in the native TAP structure to 4.7 Å in the TAP−OCA structure, thereby leading to the formation of a hydrophobic bridge across the substrate-binding crevice that covers the C^4-C^8 atoms of OCA (Figure 5b). In addition, Leu76 exhibits close contacts with Pro110 and Tyr113 (Table 3) and van der Waals interactions with the C^7 and C^8 atoms of OCA in the TAP−OCA structure (lengths of 4.2 and 4.3 Å, respectively). Switch loop movement also makes Gly75 form close contacts with Leu109, Tyr113, Tyr117, and Phe121 (Table 3). These results show that OCA binding induces switch loop movement mainly through the interactions between nonpolar carbon atoms and suggest that TAP's switch loop movement is triggered by hydrophobic interactions and Leu76 plays the pivotal role in them.

Besides these hydrophobic interactions, switch loop movement also results in six intraloop H-bonds (the main chain O−N H-bonds, Gly71−Gly75, Gly72−Leu76, Asn73−Arg77, Asp74−Arg77, Asp74−Phe79, and Gly75−Gly78) and two interloop H-bonds (the O atom of Leu76 with the OH group of Tyr113 and the O atom of Phe79 with the OH group of Tyr117) being generated in comparison with the native TAP structure. However, none of these H-bonds is located between the switch loop and OCA. This indicates that these H-bonds are possibly not the direct force for triggering switch loop movement. It is noteworthy that most of the intraloop H-bonds are involved in the formation of helix αD′. Gly72, one residue in helix αD′, is in close contact with the C^5 and C^6 atoms of OCA. Thus, the possibility of OCA binding driving the formation of helix αD′ which triggers the switch loop movement needs to be examined. However, no structural evidence shows that the OCA binding could induce a conformational change in Gly72 to generate helix αD′. Therefore, switch loop movement is not triggered through the formation of helix αD′. However, the question of why, if there are so many H-bonds in this conformation, the native protein does not adopt this conformation needs to be asked. One possible answer is waters occupy the substrate-binding crevice, which destabilizes this conformation and makes it both enthalpy and entropy unfavorable. The OCA binding depletes the water molecules and removes the destabilization factor.

Taken together, the binding of a middle or long acyl chain substrate results in a continuous hydrophobic surface, connecting the Leu11 and Pro110 hydrophobic clusters, and subsequently drives the Leu76 to interact with them and triggers switch loop movement by hydrophobic stabilizations. Switch loop movement further increases the hydrophobicity around the substrate-binding crevice. Therefore, the effect of switch loop movement could also increase the stability of a bound substrate with an acyl chain length of more than four carbons.

TAP's Switch Loop Movement Is Abolished in the L109P Mutant. The first structure of TAP determined by us was its L109P mutant (*12*). The crystal structure of the L109P mutant shows almost the same overall architecture and spatial dispositions of the catalytic triad and oxyanion acceptors as the native TAP structure with a rmsd of 0.6 Å over 178 C^α atoms. Notably, the switch loop of the L109P mutant shows an ordered conformation with a well-defined electron density, which is apparently unlike that of either native TAP or TAP−OCA. The crystallization conditions and diffraction quality of native TAP and L109P mutant crystals are very similar, and their space groups, unit cell parameters, and crystal packing are the same (*12*). Therefore, the switch loop of the L109P mutant, with a conformation different from that of native TAP, is not a crystallization artifact. In comparison to the native TAP structure, the switch loop in the L109P mutant structure is apparently stabilized by two additional main chain O−N H-bonds, from the carbonyl of G75 to the NH groups of G78 and F79, and four water-mediated interloop H-bonds, mainly connecting the residues of the switch loop and two tyrosine residues, Tyr113 and Tyr117,

in $loop_{110-120}$. In other words, $loop_{110-120}$ moves toward the switch loop to form the water-mediated H-bonds to stabilize the switch loop of the L109P mutant. It seems that Leu109 mutated to a more rigid and smaller Pro109 not only provides a space to allow movement of $loop_{110-120}$ but also coincidentally generates the binding sites for water molecules, which create the water-mediated H-bonds, which stabilize both $loop_{110-120}$ and switch loop and make both loops more rigid.

As we mentioned, Leu109 is a hydrophobic residue located at the Pro110 hydrophobic cluster of TAP and is involved in the hydrophobic interactions which trigger switch loop movement. We thus are interested in the relationship between residue 109 and the switch loop in the L109P mutant. To decipher this question, we obtained the crystals of the L109P mutant in complex with OCA. The L109P−OCA crystal structure shows us OCA lodges in the substrate-binding crevice of the L109P mutant in the same way as in native TAP. Interestingly, switch loop movement observed in the TAP−OCA structure is abolished in the L109P−OCA structure. Also, the water-mediated H-bonds stabilizing the L109P's switch loop are absent. The electron density map of the switch loop becomes disordered and the conformation of the switch loop becomes flexible in the L109P−OCA structure like that in TAP structure. These observations suggest that Leu109 is essential for OCA-induced switch loop movement. Leucine and proline differ in hydrophobicity, side chain size, and geometry, which may be the factors causing defective switch loop movement in the L109P mutant.

As for geometry, proline is more rigid than leucine. The ϕ and ψ angles of residue 109 in the native TAP and L109P mutant structures differ by 22.7° and 6.4°, respectively. Additionally, the C^{α} atom of Pro109 moves ~0.6 Å toward the cavity in comparison with that of Leu109 in native TAP due to the cavity generated between Pro109 and Phe121 in the L109P mutant. Nonetheless, when OCA binds to the L109P mutant, the temperature factors of $loop_{111-120}$ in the L109P−OCA structure increase and are comparable with those of $loop_{111-120}$ in the native TAP and TAP−OCA structures (Figure 1). In addition, a shift in $loop_{111-120}$ was observed when OCA binds to the L109P mutant as shown in Figure 2. $Loop_{111-120}$ in the L109P−OCA structure adopts a conformation similar to that in the TAP−OCA structure. These imply that $loop_{111-120}$ is still movable in the L109P mutant. Moreover, inspection of the L109P−OCA structure revealed that there is no possible steric hindrance to prevent switch loop movement. Therefore, the more rigid property of Pro109 is probably not a major factor abolishing TAP's switch loop movement.

With regard to hydrophobicity, the hydrophobicity values of leucine and proline are 3.8 and −1.6, respectively, according to the most frequently used hydrophobicity scale (*24*). Leu109 mutated to Pro109 should decrease the hydrophobicity of TAP's Pro110 hydrophobic cluster, and thus weaken the hydrophobicity of the continuous hydrophobic surface generated by OCA binding. Thus, weakened hydrophobicity around the substrate-binding crevice by the L109P substitution could be a reason OCA binding cannot induce switch loop movement in the L109P−OCA complex.

As mentioned before, Leu109 forms close contacts with Gly75 when OCA binds to native TAP. The close contacts between residue 109 and Gly75, however, no longer exist in the L109P−OCA structure because of a smaller side chain of Pro109. Also, a smaller side chain of Pro109 results in a cavity between Pro109 and Phe121, which disrupts the integrity of the hydrophobic surface of the Pro110 hydrophobic cluster in the L109P mutant (Figure 6). Therefore, a shorter side chain of Pro109 could also be a reason that switch loop movement is abolished in L109P−OCA complex.

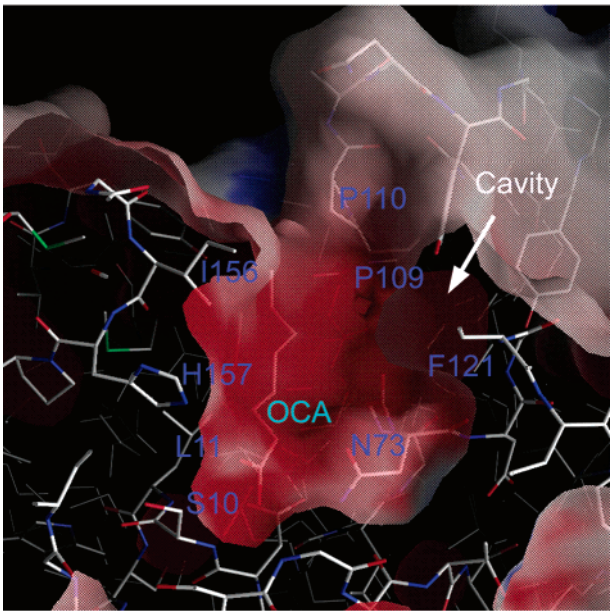

FIGURE 6: GRASP presentation of the electrostatic potential surface of L109P−OCA. The cavity generated between Pro109 and Phe121 in the L109P−OCA structure is indicated.

When OCA binds to L109P, $loop_{111-120}$ tries to move toward the binding crevice, and this withdraws two tyrosine residues and abolishes four water-mediated H-bonds. With the balance of OCA binding driving force on one side and L109P switch loop stabilization forces on the other side, the L109P−OCA complex acts like native TAP around the switch loop, which is flexible and has high *B* factors. In conclusion, the hydrophobicity of Leu109 and the length of its side chain are critical for TAP's switch loop movement. These results also support our aforementioned elucidation that TAP's switch loop movement is induced by hydrophobic interactions.

Role of the Switch Loop in the Catalytic Mechanism of TAP. The L109P mutant has an alternative substrate specificity profile compared to that of wild-type TAP, which was originally thought to be caused by its C-terminal His_6 tag (*16*). However, when the L109P structure was determined, it was found that the C-terminal His_6 tag could not possibly interfere with the substrate-binding crevice due to steric hindrance (*12*). Therefore, the differences in substrate specificity between wild-type TAP and its L109P mutant may be caused by the mutation at residue 109. Nevertheless, our structures show that residue 109 is not in close contact with OCA. In addition, residue 109 is buried under Gly75 by switch loop movement (Figure 5b). These facts suggest that the L109P mutation may not significantly affect TAP's substrate binding affinity. This hypothesis is supported by previous enzyme kinetic analyses showing that native TAP and its L109P mutant display comparable K_m values for C_{16}-CoA, *p*-nitrophenyl dodecanoate (C_{12}), and *p*-nitrophenyl

Table 4: Kinetic Parameters for Wild-Type TAP (WT-TAP) and Its L109P Mutant (L109P)[a]

	WT-TAP			L109P			
substrate	K_m (μM)	k_{cat} (s^{-1})	k_{cat}/K_m ($s^{-1}\,\mu M^{-1}$)	K_m	k_{cat} (s^{-1})	k_{cat}/K_m ($s^{-1}\,\mu M^{-1}$)	$\Delta\Delta G^*$ [b] (kJ/mol)
thioester							
palmitoyl-CoA	6.38	19.1	2.99	5.95	2.46	0.413	5.09
ester							
p-nitrophenyl dodecanoate	1448.6	10.2	0.007	1312.3	0.9	0.0007	5.93
p-nitrophenyl hexanoate	1360.3	30.5	0.022	1690.0	50.2	0.03	−0.80

[a] From ref *16*. [b] $\Delta\Delta G^*$ is the change in the free energy of transition state stabilization. $\Delta\Delta G^* = -RT \ln[(k_{cat}/K_m)_{L109P}/(k_{cat}/K_m)_{WT-TAP}]$.

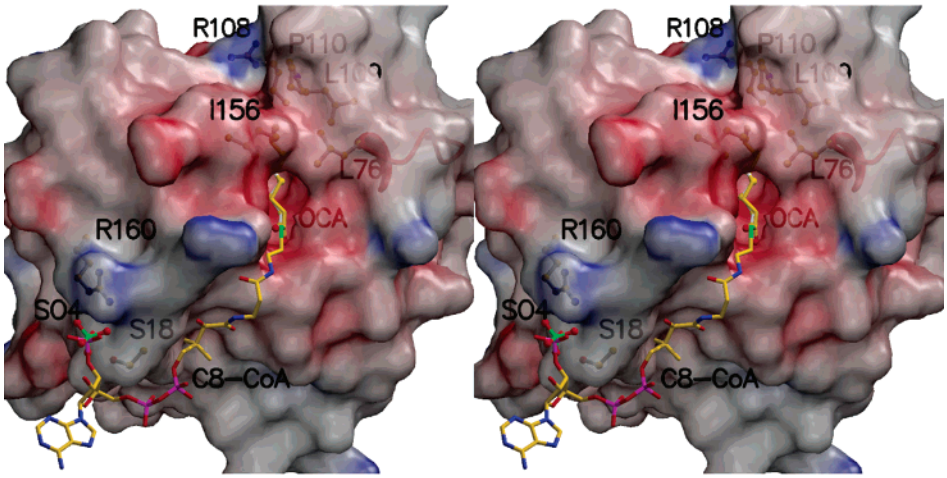

FIGURE 7: Putative CoA binding site of TAP. A stereoview of the molecular surface of the TAP−OCA structure is presented with positive (blue) and negative (red) electrostatic potential. The diagram shows a C8-CoA model in the putative CoA binding site of the TAP−OCA structure. The C8-CoA model was generated using O and subjected to energy minimization using CNS. C8-CoA is shown as sticks, while OCA and a sulfate ion are shown as balls and sticks.

hexanoate (Table 4) (*16*). In this study, we have shown that the L109P mutation abolished switch loop movement induced by OCA binding. We thus are interested in how Leu109 was mutated to Pro109 and the consequent defect in switch loop movement affects the substrate specificity of TAP.

In general, the catalytic efficiency of an enzyme is determined by its ability to stabilize the transition state intermediates and is best defined by the k_{cat}/K_m ratio. Previous enzyme kinetic analyses showed that the k_{cat}/K_m values of the L109P mutant for two long acyl chain substrates, C_{16}-CoA and *p*-nitrophenyl dodecanoate (C_{12}), are 7.2- and 10-fold lower than those of wild-type TAP, respectively (Table 4) (*16*). By contrast, for a middle acyl chain substrate, *p*-nitrophenyl hexanoate, the k_{cat}/K_m values of wild-type TAP and its L109P mutant are very similar (Table 4) (*16*). These results reveal that the L109P mutation decreases TAP's catalytic efficiency for long acyl chain substrates, not middle acyl chain substrates. This also means that the L109P mutation could decrease the stability of the transition state intermediates of long acyl chain substrates, not middle acyl chain substrates. In the TAP−OCA structure, residue 109 is buried under Gly75 by switch loop movement (Figure 5b). Thus, the possibility that residue 109 directly stabilizes the transition state intermediates can be ruled out due to steric hindrance. However, the switch loop joins and expands the continuous hydrophobic surface of the substrate-binding crevice, which could provide additional force to stabilize transition state intermediates. Therefore, the decreasing catalytic efficiency of the L109P mutant for long acyl chain substrates could result from the defect in switch loop movement.

Notably, the switch loop is not in close contact with the catalytic triad and oxyanion acceptors of TAP. This reveals that the role of the switch loop could not be to stabilize a tetrahedral oxyanion intermediate. This is also supported by the fact that the L109P mutation does not alter TAP's catalytic efficiency for middle acyl chain substrates. In addition, the calculated activation energy in the L109P mutant significantly increases by 5.09 and 5.93 kJ/mol for C_{16}-CoA and *p*-nitrophenyl dodecanoate, respectively, when compared to that of wild-type TAP (Table 4) (*16*). In contrast, the calculated activation energy for middle acyl chain substrates is very similar in wild-type TAP and the L109P mutant. Because the enhancement of catalytic efficiency can be contributed by the binding energy of Michaelis complex (MC) formation, we thus propose that the effect of switch loop movement in TAP's catalytic mechanism could be to stabilize the TAP−substrate complex (as a MC). Also, switch loop movement is essential for TAP's substrate preference for the long acyl chain substrate molecules.

Enzymes in catalysis use numerous detailed chemical mechanisms to achieve transition state stabilization. The studies on the catalytic efficiency and major catalytic power of enzymes are focused mainly on the stabilization of tetrahedral intermediates. Herein, we provide valuable structural evidence for elucidating MC stabilization, a less discussed step in the catalytic mechanisms of serine hydrolases and SGNH-hydrolases, by TAP's switch loop, which enhances TAP's catalytic efficiency.

Putative CoA Binding Site. The TAP−OCA structure reported here identified a crevice for acyl chain binding.

However, enzyme kinetic analyses revealed that TAP shows apparently different binding affinity for long acyl thioesters and long acyl esters (*9*, *16*). TAP's K_m values are ~7 μM for C_{16}-CoA and >1000 μM for *p*-nitrophenyl esters. The difference in the substrate binding affinity of TAP for C_{16}-CoA and *p*-nitrophenyl esters probably results from their different alcohol moieties, CoA and *p*-nitrophenol, respectively. A CoA moiety, comprised of pantetheine, adenosine, and phosphoric acid, may make more contacts with TAP than a *p*-nitrophenol moiety does. Although there is no apparent CoA binding pocket in the TAP structures, a sulfate ion was found at the surface of the TAP structures and hydrogen bonded to Ser18 and the positively charged Arg160 of TAP. Moreover, the location of the sulfate ion and the distance between the sulfate ion and the catalytic residues in the TAP structure allow us to model an octanoyl-CoA (C8-CoA) in the TAP structure (Figure 7). Thus, the sulfate ion may be comparable to the phosphate portion of CoA. These data imply that TAP could have a CoA binding site besides a substrate-binding crevice for acyl moieties. We also propose that residues Ser18 and Arg160 could be involved in CoA recognition or binding.

In addition, Karasawa et al. (*23*) have reported that the reaction rate declines to one-eighth at substrate concentrations greater than 1 mM in the hydrolysis of palmitoyl-CoA, a phenomenon known as negative feedback. The observed negative feedback in the hydrolysis of palmitoyl-CoA (*23*) could be explained by substrate inhibition in that two substrate molecules may bind to different subsites of the enzyme active site when the concentration of the substrates is high. This result could support our prediction that TAP has a CoA binding site besides a substrate-binding crevice for acyl moieties. This could also explain why the catalytic efficiencies of TAP for *p*-nitrophenyl esters with the long acyl chain length are significantly lower than that for palmitoyl-CoA (*9*, *16*), because the CoA binding site helps to stabilize the transition state intermediates of thioesters with long acyl chains, thereby enhancing the catalytic efficiency.

In this study, we have shown that OCA induces TAP's switch loop movement by increasing the hydrophobicity of the substrate-binding crevice. Together with previous enzyme kinetic analyses, we suggest that the effect of switch loop movement is to stabilize the TAP−substrate complex (MC) during catalysis and that the switch loop movement is essential for TAP's substrate preference for thioesters with long acyl chains. Structural analyses of the L109P mutant also support this hypothesis. In the serine hydrolases with typical catalytic triads of known structures, the best known flexible loop movement is observed in fungal lipases. In the close form of the lipases, a surface loop, called flap or lid, shields the active site of the lipases from the solvent. When it encounters an oil−water interface, the flap displays a drastically conformational movement to expose the buried active site under the flap and, in some cases, to rearrange the position of the oxyanion acceptors to accommodate substrates, a phenomenon known as interfacial activation. However, TAP does not display interfacial activation. The active site of TAP is preformed and exposed to the solvent. Also, TAP's switch loop moves toward the substrate-binding crevice to interact with the substrate. Past reports have shown that some lipases, esterases, or thioesterases do not display interfacial activation and also do not have a lid domain or switch loop governing substrate binding. Switch loop movement is unobserved in these enzymes because a suitable enzyme−substrate complex is not available or crystal contacts prevent such a movement. Thus, TAP's switch loop movement reported here, with significant differences compared to those of lipases, would be a possible step in the catalytic mechanism of those enzymes. So far, there is no structural evidence for elucidating such a new relationship between the flexible loop movement and the catalytic efficiency of serine hydrolases for long acyl chain substrates. This study provides valuable insights into understanding TAP's catalytic mechanism, a mechanism which is novel in the lipolytic enzymes and thioesterases.

ACKNOWLEDGMENT

We thank one reviewer who gave us many valuable suggestions. We are grateful to Dr. Kenrick Deen for critical reading and comments concerning the manuscript. We acknowledge Dr. Hideaki Moriyama for assistance with the TAP−OCA data collection, which was carried out at SPring-8 in cooperation with the Japan Synchrotron Radiation Research Institute. The L109P−OCA data collection was based upon research conducted at the NSRRC, Taiwan.

REFERENCES

1. Derewenda, Z. S., and Wei, Y. (1995) Molecular mechanism of enantiorecognition by esterases, *J. Am. Chem. Soc. 117*, 2104−2105.
2. Jaeger, K.-E., and Reetz, M. T. (1998) Microbial lipases form versatile tools for biotechnology, *Trends Biotechnol. 16*, 396−403.
3. Arpigny, J. L., and Jaeger, K.-E. (1999) Bacterial lipolytic enzymes: Classification and properties, *Biochem. J. 343*, 177−183.
4. Jaeger, K.-E., Dijkstra, B. W., and Reetz, M. T. (1999) Bacterial biocatalysts: Molecular biology, three-dimensional structures, and biotechnological applications of lipases, *Annu. Rev. Microbiol. 53*, 315−351.
5. Barnes, E. M., Jr., and Wakil, S. J. (1968) Studies on the mechanism of fatty acid synthesis, *J. Biol. Chem. 243*, 2955−2962.
6. Pacaud, M., and Uriel, J. (1971) Isolation and some properties of a proteolytic enzyme from *Escherichia coli* (Protease I), *Eur. J. Biochem. 23*, 435−442.
7. Albright, F. R., White, D. A., and Lennarz, W. J. (1973) Studies on enzymes involved in the catabolism of phospholipids in *Escherichia coli*, *J. Biol. Chem. 248*, 3968−3977.
8. Karasawa, K., Kudo, I., Kobayashi, T., Homma, H., Chiba, N., Mizushima, H., Inoue, K., and Nojima, S. (1991) Lysophospholipase L_1 from *Escherichia coli* K-12 overproducer, *J. Biochem. 109*, 288−293.
9. Lee, Y. L., Chen, J. C., and Shaw, J. F. (1997) The thioesterase I of *Escherichia coli* has arylesterase activity and shows stereospecificity for protease substrates, *Biochem. Biophys. Res. Commun. 231*, 452−456.
10. Cho, H., and Cronan, J. E., Jr. (1993) *Escherichia coli* thioesterase I, molecular cloning and sequencing of the structural gene and identification as a periplasmic enzyme, *J. Biol. Chem. 268*, 9238−9245.
11. Doi, O., and Nojima, S. (1975) Lysophospholipase of *Escherichia coli*, *J. Biol. Chem. 250*, 5208−5214.
12. Lo, Y. C., Lin, S. C., Shaw, J. F., and Liaw, Y. C. (2003) Crystal structure of *Escherichia coli* Thioesterase I/Protease I /Lysophospholipase L_1: Consensus sequence blocks constitute the catalytic center of SGNH-hydrolases through a conserved hydrogen bond network, *J. Mol. Biol. 330*, 539−551.
13. Wei, Y., Schottel, J. L., Derewenda, U., Swenson, L., Patkar, S., and Derewenda, Z. S. (1995) A novel variant of the catalytic triad in the *Streptomyces scabies* esterase, *Nat. Struct. Biol. 2*, 218−223.

14. Ho, Y. S., Swenson, L., Derewenda, U., Serre, L., Wei, Y., Dauter, Z., Hattori, M., Adachi, T., Aoki, J., Arai, H., Inoue, K., and Derewenda, Z. S. (1997) Brain acetylhydrolase that inactivates platelet-activating factor is a G-protein-like trimer, *Nature 385*, 89−93.
15. Molgaard, A., Kauppinen, S., and Larsen, S. (2000) Rhamnogalacturonan acetylesterase elucidates the structure and function of a new family of hydrolases, *Structure 8*, 373−383.
16. Lee, Y. L., Su, M. S., Huang, T. H., and Shaw, J. F. (1999) C-Terminal His-tagging results in substrate specificity changes of the thioesterase I from *Escherichia coli*, *J. Am. Oil Chem. Soc*. *76*, 1113−1118.
17. Otwinowski, Z., and Minor, W. (1997) Processing of X-ray Diffraction Data Collected in Oscillation Mode, *Methods Enzymol*. *276*, 307−326.
18. Brunger, A. T., Adams, P. D., Clore, G. M., DeLano, W. L., Gros, P., Grosse-Kunstleve, R. W., Jiang, J. S., Kuszewski, J., Nilges, M., Pannu, N. S., et al. (1998) Crystallography and NMR system: A new software system for macromolecular structure determination, *Acta Crystallogr. D54*, 905−921.
19. Laskowski, R. A., MacArthur, M. W., Moss, D. S., and Thornton, J. M. (1993) PROCHECK: A program to check the stereochemical quality of protein structures, *J. Appl. Crystallogr*. *26*, 283−291.
20. Jones, T. A., Zou, J. Y., Cowan, S. W., and Kjelgaard, M. (1991) Improved methods for building protein models in electron density maps and the location of errors in these models, *Acta Crystallogr. A47*, 110−119.
21. McDonald, I. K., and Thornton, J. M. (1994) Satisfying hydrogen bonding potential in proteins, *J. Mol. Biol*. *238*, 777−793.
22. Wallace, A. C., Laskowski, R. A., and Thornton, J. M. (1995) LIGPLOT: A program to generate schematic diagrams of protein−ligand interactions, *Protein Eng*. *8*, 127−134.
23. Karasawa, K., Yokoyama, K., Setaka, M., and Nojima, S. (1999) The *Escherichia coli pld*C gene encoding lysophospholipase L_1 is identical to the *ape*A and *tes*A genes encoding protease I and thioesterase I, respectively, *J. Biochem*. *126*, 445−448.
24. Kyte, J., and Doolittle, R. F. (1982) A simple method for displaying the hydropathic character of a protein, *J. Mol. Biol*. *157*, 105−132.
25. Collaborative Computational Project, Number 4 (1994) The CCP4 suite: Programs for protein crystallography, *Acta Crystallogr. D50*, 760−763.
26. Merritt, E. A., and Bacon, D. J. (1997) Raster3D: Photorealistic molecular graphics, *Methods Enzymol*. *277*, 505−524.
27. Arnez, J. G. (1994) MINIMAGE: A program for plotting electron density maps, *J. Appl. Crystallogr*. *27*, 649−653.
28. Nicholls, A., Sharp, K., and Honig, B. (1991) Protein folding and association: Insights from the interfacial and thermodynamic properties of hydrocarbons. *Proteins 11*, 281−296.

BI048109X